EUROFUSION WPJET1-CP(16) 15124

CF Maggi et al.

Studies of the pedestal structure in JET with the ITER-like wall

Preprint of Paper to be submitted for publication in
Proceedings of 26th IAEA Fusion Energy Conference

This work has been carried out within the framework of the EUROfusion Consortium and has received funding from the Euratom research and training programme 2014-2018 under grant agreement No 633053. The views and opinions expressed herein do not necessarily reflect those of the European Commission.

Studies of the pedestal structure in JET with the ITER-like wall

CF Maggi[1], L Frassinetti[2], L Horvath[3], A Lunniss[3], S Saarelma[1], H Wilson[3], FJ Casson[1], E Delabie[4], M Leyland[3], I Lupelli[1], S Pamela[1], H Urano[5] and JET Contributors*

EUROfusion Consortium, JET, Culham Science Centre, Abingdon, OX14 3DB, UK
[1]CCFE, Culham Science Centre, Abingdon OX14 3DB, UK
[2]Association VR, Fusion Plasma Physics, KTH, SE-10044 Stockholm, Sweden
[3]York Plasma Institute, Department of Physics, University of York, York YO10 5DD, UK
[4]Oak Ridge National Laboratory, Oak Ridge, Tennessee, US
[5]National Institutes for QST, Naka, 311-0193, Japan
**See the author list of "Overview of the JET results in support to ITER" by X. Litaudon et al. to be published in Nuclear Fusion Special issue: Overview and summary reports from the 26th Fusion Energy Conference (Kyoto, Japan, 17-22 October 2016)*

First author's email address: Costanza.Maggi@ukaea.uk

Abstract. The pedestal structure of type I ELMy H-modes has been analysed for JET-ILW. The electron pressure pedestal width is independent of ρ^* and increases proportionally to $\sqrt{\beta_{pol,PED}}$. Additional broadening of the width is observed, at constant $\beta_{pol,PED}$, with increasing ν^* and/or neutral gas injection, thus the contribution of atomic physics effects in setting the width cannot as yet be ruled out. Neutral penetration alone does not determine the shape of the density profile. The inter-ELM temporal evolution of the pedestal structure is not unique, but depends on discharge conditions. At low gas injection, $p_{e,PED}$ increases during the ELM cycle due steepening of the gradient at constant or moderately narrowing width. The strong reduction in $p_{e,PED}$ with increasing D_2 gas injection at higher power is primarily due to clamping of ∇T_e, half way through the ELM cycle and is suggestive of turbulence limiting the T_e pedestal growth, while the n_e pedestal can still develop inter-ELM. The peak edge bootstrap current j_{BS} increases during the ELM cycle, both at low and high beta, at low gas injection, while it is much reduced and remains roughly constant throughout the ELM cycle with increasing D_2 gas rate ($/\nu^*_{PED}$). First results of recent isotope experiments in H and D show reduced energy and particle confinement in H H-modes. The power threshold for type I/type III ELMs roughly doubles from D to H.

1. Introduction

Recent pedestal studies in JET have focussed on the characterization of the H-mode pedestal structure with the ITER-like Be/W wall (JET-ILW), in which the pedestal evolution is limited by type I ELMs. The datasets analysed, unless otherwise stated, are systematic power scans at 1.4MA/1.7T at 3 levels of D_2 gas rate: $3\text{x}10^{21}$ e/s ("low"), $8\text{x}10^{21}$ e/s ("medium") and $1.8\text{x}10^{22}$ e/s ("high") [1]. Recent experiments extended the dataset to lower power to map empirically the type I/type III ELM boundary. This lies just above the L-H threshold power, P_{L-H}, and therefore is at reduced pedestal temperature, $T_{e,PED}$, compared to JET with the Carbon wall (JET-C). As previously reported, P_{L-H} is lower in JET-ILW in the high density branch [2]. Figure 1 summarizes the data with $T_{e,PED} - n_{e,PED}$ diagram (a) and with ELM frequency f_{ELM} vs P_{sep} (b), with P_{sep} the net power across the separatrix. The dataset connects to the hybrid scenario at low gas rate/high beta and to the high I_P baseline scenario (albeit at lower I_P/B_T) at high gas rate/medium-low beta. Because of the relatively low I_P/B_T of this dataset, a variation in beta of a factor of 2 could be achieved in the type I ELMy regime.

2. Characterization of the pedestal structure and pedestal parameters

The electron pedestal structure is characterized in geometrical form by the height, gradient and width of the pedestal region. It is measured primarily using High Resolution Thomson Scattering (HRTS), with a sampling frequency of 20 Hz. When available, the T_e profile

measurements are supported by high time resolution ECE data (0.4 ms) and the n_e profiles by Li-beam (~ 15 ms) and reflectometry data (sampling rate > 15 μs). The ion pressure p_i cannot be characterized to this detail, so we focus on p_e in this work. For a given discharge, the HRTS profiles collected from a steady time window are ELM-syncronized to form a composite profile and the ELM cycle is divided into 20% long intervals. The parameters for density (n_e), temperature (T_e) and pressure (p_e) are evaluated by means of modified hyperbolic tangent function fits to the respective profiles. The first ELM interval, 0-20%, is ignored, as it is at times affected by the ELM crash phase. The pre-ELM quantities are those relating to the 80-99% ELM interval and are used for the pedestal width scaling studies.

Edge pressure gradient and edge current density are the two key parameters that determine the pedestal stability. The current density in the pedestal is dominated by the bootstrap current, j_{BS}, primarily driven by the edge pressure gradient, but also strongly influenced by the edge collisionality, ν*. The edge j_{BS} profile is derived with the local neoclassical transport code NEO [3], [4], which solves the drift-kinetic equation with a full linearized Fokker-Planck collision operator including all inter-species collisions. This allows for a more accurate estimate of j_{BS} than using the Sauter formula [5], [6], especially in JET pedestals at high ν*, where j_{BS}(Sauter) has been shown to overestimate j_{BS}(NEO) by up to a factor of two [1]. The input to NEO are the EFIT plasma equilibrium, the electron kinetic profiles (T_i is assumed equal to T_e) and the line averaged Z_{eff} (measured from visible Bremsstrahlung) to evaluate the ion density, with Be as the intrinsic impurity. The sensitivity of the derived j_{BS} to the uncertainties of the measured n_e, T_e and Z_{eff} have been evaluated using modulated input profiles, as described in [7].

3. Pedestal width scaling

Similarly to what is observed in several tokamaks, including JET-C, in JET-ILW the pre-ELM electron pedestal pressure width $\Delta_{pe}(\psi)$ increases with pedestal poloidal beta, $\beta_{pol,PED}$, in ψ space, proportionally to $\sqrt{\beta_{pol,PED}}$ [1], as assumed in the EPED model [8]. The pedestal broadening in ψ space can be associated with the increase in Shafranov shift, which stabilizes the ballooning modes [9], [10].

On the other hand, high δ pedestals at high D_2 injection rates – a necessary condition in JET-ILW to enable steady H-mode conditions compatible with core W control over longer time scales - are not fully consistent with the EPED model assumptions. In these plasmas the pedestal widens at constant $\beta_{pol,PED}$ but with increasing pedestal collisionality, $\nu^*_{PED,}$ thus deviating from the KBM-based dependence of the pedestal width posited in the model [11]. In recent dimensionless H-mode experiments at low δ, where ν^*_{PED} was varied by a factor of 5 at constant q_{95}, normalized ion Larmor radius ρ* and normalized thermal β, $\Delta_{pe}(\psi)$ broadens at constant $\beta_{pol,PED}$ with increasing $\nu^*_{PED.}$ Regression to the data shows $\Delta_{pe}(\psi) \sim (\beta_{pol,PED})^{0.5} (\nu^*_{PED})^{0.26}$ [12]. In contrast, in the dimensional power and gas scan experiments, which resulted in a factor of 10 variation in ν^*_{PED}, $\Delta_p(\psi) / \sqrt{\beta_{pol,ped}}$ is constant with $\nu^*_{PED,}$ but is systematically wider at higher than at lower D_2 gas rates at a given value of ν^*_{PED} [1]. As $\beta_{pol,PED}$ and ν^*_{PED} are correlated in the dimensional power and gas scans, a subset of the data is selected in the narrow interval of $0.185 < \beta_{pol,PED} < 0.22$, which has sufficient variation of ν^*_{PED} at ~ constant $\beta_{pol,PED}$. The pedestal width, normalized to the scaling derived in the dimensionless ν* scan, shows a residual increase in normalized Δ_{pe} with D_2 gas rate (assumed as proxy for the neutral source, as fuelling from neutral beam injection is negligible). Therefore, the combined results of the dimensional and dimensionless experiments do not necessarily indicate a dependence of $\Delta_{pe}(\psi)$ on ν*, in addition to that on $\sqrt{\beta_{pol,PED}}$. Rather, they may be indicative of an additional dependence of the pedestal width on

parameters either directly or indirectly connected with the D neutral content in the plasma, implying that atomic physics effects could also contribute in setting the pedestal width.

The neutral penetration model for the density width [13] assumes the shape of the n_e profile to be determined by edge fuelling and constant diffusion, with the width of the edge transport barrier being proportional to the neutral penetration length. In its simplest formulation, if charge exchange processes are neglected, the model predicts $\Delta_{ne} \sim 1/n_{e,PED}$, which can quickly be tested against the experimental pedestal widths to check whether the model captures the main trend in the data. Comparison to JET-ILW n_e widths indicates that for some datasets Δn_e is broadly consistent with the neutral penetration model predictions, as shown in Figure 2a for a low δ dataset of type I ELMy H-modes with I_P = 1.4 – 4.0 MA and B_T = 1.7 – 3.7T. Note that it's charge exchange (CX) processes that allow neutral penetration inside the LCFS at high pedestal density, so this effect needs to be taken into account for more quantitative comparisons. Saturation of the n_e width to a constant value at high $n_{e,PED}$ (Figure 2a) may indicate CX setting neutral penetration at high density. However, the model is too simple and does not capture all the physics of the wider database, as indicated in Figure 2b for two datasets at high δ (note that it is not necessarily implied here that the reason for the discrepancy is ascribed to the difference in plasma triangularity in the two datasets, as this may be purely coincidental). The dashed black curves in Figures 2a and 2b indicate a variation of $\Delta_{ne} \sim 1/n_{e,PED}$. Both the power scan at 1.4MA/1.7T (orange triangles, from experiments in [1]) – with Δ_{ne} increasing at constant $n_{e,PED}$ - and the D_2 gas scan at constant power at 2.5MA/2.65T (red stars, from experiments in [11]) deviate strongly from the simple approximation of the model. Another dataset which is at odds with the neutral penetration model assumptions is that of dimensionless ν^* scans discussed in [12], which exhibit substantial broadening of Δ_{ne} at roughly constant $n_{e,PED}$. In summary, neutral penetration alone does not appear to set the n_e width in JET-ILW. Therefore, a combination of source and transport effects is likely to set the shape of the pedestal n_e profile in JET-ILW, as pointed out in an earlier analysis for AUG data [14]. It is possible that, depending on the discharge conditions, neutral penetration effects may become dominant compared to transport effects. One such example may be the n_e width variation in the datasets of Figure 2a and 2b discussed above (although the underlying physics reason remains as yet unexplained). A physics model for the pedestal density that captures all conditions of the operating space is still outstanding and is an important element for achieving full predictive capability of the pedestal height.

Finally, dimensionless scans in ρ^*, with constant q_{95}, ν^* and thermal β, have confirmed the absence of a sizeable scaling of $\Delta_{pe}(\psi)$ with ρ^* [15], consistently with earlier findings in JET-C/DIII-D experiments [16] and in other tokamaks. Moreover, also the normalized pressure gradient does not depend on ρ^*, within the uncertainty in the data. These findings project favourably to ITER operation.

4. Pedestal evolution during the type I ELM cycle

The temporal evolution of the pedestal parameters during the ELM cycle is studied to understand how the ELM trigger is reached under varying experimental plasma discharge conditions, notably as a function of β_N and D_2 gas injection. If Kinetic Ballooning Modes (KBMs) are assumed to control the pressure gradient evolution during the type I ELM cycle, as within the EPED model framework, the build-up of the pedestal should occur first with the pedestal pressure gradient growing unconstrained until the KBM boundary is reached, and subsequently with p_{PED} increasing through widening of the pedestal pressure width Δp at fixed gradient, until the Peeling-Ballooning (P-B) boundary is reached and the type-I ELM is triggered. Note that a study of JET-C high δ H-modes found, at low gas injection, the

pedestal height to increase due to steepening of the pressure gradient and narrowing of the pressure width during the inter-ELM pedestal recovery phase, in contrast to the pedestal gradient being limited by KBMs [17]. The inter-ELM pedestal evolution in JET-ILW is found to vary with plasma conditions, often in a complex fashion, and is generally not consistent with the assumptions underpinning the EPED model.

Power scans at low D_2 gas injection: *the pre-ELM edge stability, calculated with Helena/ELITE, is consistent with the P-B model throughout the beta scan [1]: the EPED model P-B constraint is satisfied.*

$n_{e,PED}$ decreases with power (/β_N), roughly by 30% overall, as f_{ELM} increases with power at constant D_2 gas rate, and it grows monotonically during the ELM cycle. At the highest β_N, Δn_e narrows and ∇n_e steepens until the ELM occurs, suggesting qualitative consistency with the neutral penetration model. The density gradient is larger at low β_N. $T_{e,PED}$ increases substantially with power but, unlike $n_{e,PED}$, it remains largely constant in the second half of the ELM cycle, except at the highest power ($\beta_N = 2.8$), where it grows monotonically till the ELM crash. At low/medium power the increase in ∇T_e compensates the narrowing of the width. At $\beta_N = 2.8$ $T_{e,PED}$ grows due to steepening of the gradient at constant width (Figure 3a). The temperature width is broader and the gradient steeper at high β_N. As a result, $p_{e,PED}$ increases with power (2x overall in the power scan) and grows throughout the ELM cycle, in particular at the highest β_N, due to steepening of the gradient (Figure 4a) at constant or moderately narrowing width (Figure 4b). The peak j_{BS} continuously increases during the ELM cycle, both at low and high β_N [7]. The observed inter-ELM growth of the electron pedestal pressure is not consistent with instabilities clamping the pressure gradient during the ELM cycle and with a subsequent growth of $p_{e,PED}$ due to broadening of Δ_{pe}, as posited in EPED. Therefore, the pedestal p_e evolution at low D_2 gas injection is consistent with the P-B constraint, but not consistent with the KBM constraint.

Power scans at high D_2 gas injection: *at high gas rates, the pre-ELM edge stability is consistent with the ELMs being triggered by P-B modes at low β_N, but it predicts the pedestal to be deeply stable to P-B modes at high β_N [1]. Although the ELMs are empirically identified as being of type I with the power scan, they are different in character compared to type I ELMs at low gas rates [1]. This discrepancy between P-B model and experiment points to missing physics for the ELM instability onset. The EPED model P-B constraint is satisfied at low β_N, but is not satisfied at higher β_N.*

As in the low gas case, $n_{e,PED}$ decreases with power/f_{ELM} and grows monotonically during the ELM cycle. As the D_2 gas rate increases at constant power, $T_{e,PED}$ is degraded compared to the low gas case, in particular at higher power. At the highest power in the scan ($\beta_N = 2$) $T_{e,PED}$ saturates half way through the ELM cycle, due to clamping of ∇Te at constant width (Figure 4b). Therefore, the reduction in $p_{e,PED}$ with increasing D_2 gas injection measured in JET-ILW at higher β_N, at constant net input power [1], is primarily due to the clamping of $T_{e,PED}$ half way through the ELM cycle. This is suggestive of turbulence limiting the T_e pedestal growth, while the n_e pedestal can still develop. At low β_N the pressure height increases during the ELM cycle, initially due to steepening of the gradient and narrowing of the width, followed by a reduction in ∇pe and a moderate increase in Δ_{pe} (Figures 5a and 5b). Therefore, the inter-ELM build-up of $p_{e,PED}$ at low β_N and high gas rate could be consistent with the EPED model assumptions, since the P-B constraint is satisfied and the pedestal evolution in the last part of the ELM cycle suggest qualitative agreement with the KBM constraint. At the highest β_N achieved at high gas rate, $\beta_N = 2$, $p_{e,PED}$ increases inter-ELM, initially due to steepening of the gradient at constant width, followed by Δ_{pe} moderately

broadening at constant gradient in the second half of the ELM cycle (Figures 5a and 5b). The inter-ELM growth of $p_{e,PED}$ is thus qualitatively consistent with that of the KBM constraint. However, the pressure evolution at high β_N and high gas rate is not consistent with the EPED model assumptions, as the P-B constraint is not satisfied. For JET pedestals, the $n = \infty$ ideal MHD ballooning limit is found to be a good proxy for KBMs in linear GK calculations [17]. For the pedestals of the power and gas scans reported in this study, and in all phases of the ELM cycle, the experimental maximum pressure gradient is always found below the $n = \infty$ ideal MHD ballooning limit and never exceeds it. This could be interpreted as indicative of the presence of KBM turbulence limiting the pressure gradient. Alternatively, it could indicate that KBMs are present in subdominant form, without limiting the growth of the pressure gradient, as in the case of the power scan at low gas injection. In the pedestals at high gas rate and higher β_N, where ∇_{Te} is clamped half way through the ELM cycle, other instabilities would thus be responsible for limiting the growth of the pedestal height. Non-linear GK analyses of these pedestals are therefore required to answer these questions. In parallel, experimental identification of the nature of the turbulence driving the residual pedestal transport inter-ELM should also be pursued.

With increasing D_2 gas rate (and thus increasing $\nu^*_{PED,}$ primarily due to the reduction in temperature) the peak j_{BS} value is much reduced and remains roughly constant throughout the ELM cycle [7]. Saturation of j_{BS} during the ELM cycle at high gas rates had also been found in JET-C [17]. In the dataset, the peak j_{BS}, the maximum pressure gradient and the maximum temperature gradient follow a similar time evolution during the ELM cycle, regardless of the time evolution of the maximum density gradient ∇n_e [7], suggesting that ∇T_e is the main drive for ∇p_e and j_{BS}. Therefore, avoiding saturation of the temperature gradient as the pedestal rebuilds in between ELM crashes is crucial to maximizing pedestal performance. The edge bootstrap current has been assumed in this study to evolve in time during the ELM cycle without delay with respect to the build-up of ∇p_e. In first order this assumption is justified by the relatively short resistive time scale for current diffusion in the edge transport barrier, $\tau_{R,}$ for the low I_P, power and gas scan dataset, characterized by relatively low $T_{e,PED}$ (for JET). A simple estimate for an effective $\tau_R = \mu_0 (\Delta_{PED})^2/\eta_{NC}$ (assuming an average ETB width Δ_{PED} = 2 cm and evaluating the neoclassical resistivity η_{NC} at the location of the maximum ∇T_e) yields $\tau_R \sim 0.1 \times \tau_{ELM}$, where τ_{ELM} is the ELM period, for both low and high ν^* pedestals of the power and gas scans [7]. It is therefore unlikely that a time delay in j_{BS} with respect to ∇p_e evolution would account for the discrepancy between P-B model and experiment for the high β_N discharges at high gas rates reported in [1].

5. Isotope effects

One of the main thrusts of recent and upcoming JET experiments is the study of isotope effects of core and pedestal in a series of campaigns in D, H and T plasmas, complementing and leading to D-T experiments with the ILW. Very recently, new isotope experiments have addressed for the first time the confinement and pedestal properties of H vs D H-modes in JET-ILW, with improved edge diagnostic capabilities compared to isotope experiments in JET-C in the late 90's. A few, preliminary highlights are given here. The plasmas were predominantly heated by NBI and had an isotope purity of 100% in D and > 97% in H. Due to the limited NB power available in H (10 MW) and the increased L-H threshold from D to H plasmas, steady type I ELMy H-modes could only be achieved in H at low I_P/B_T: at 1MA/1T, both at low and high δ, with $H_{98(y,2)} \sim 1.0 - 1.2$ and $\beta_N \sim 1.4$ - 2.5, and at 1.4MA/1.7T, low δ, with $H_{98(y,2)} \sim 1$- 1.2 and $\beta_N \sim 1.3 - 1.8$, with additional RF heating (H majority, 2nd harmonic heating at 51 MHz, up to 6.5 MW). The energy confinement is strongly reduced in H and a doubling approximately of P_{sep} is required in H to achieve

similar thermal stored energies, W_{th}, as in D. The power threshold for type I/type III ELMs, characterized by systematic power and gas variations to complement the D dataset, also doubles from D to H (Figure 6a, for 1.4MA/1.7T data). A distinct feature of H is the lower plasma density and stronger fuelling efficiency compared to D. In type I ELMy H-modes the ELM frequency is higher in H than in D at similar P_{sep} and H_2 ($/D_2$) gas rates. With both isotopes the plasma density decreases with increasing f_{ELM}, but f_{ELM} is systematically higher and the density is systematically lower in H (Figure 6b). This effect alone is unlikely to explain the lower density in H H-modes, as the density is lower also in L-mode. Therefore, it is possible that H plasmas are characterized also by degraded particle confinement compared to D. H-modes at the same W_{th} in H and D do not have matched n_e and T_e profiles: in H the lower density is compensated by higher temperature. This contrasts to JT-60U H vs D H-modes, where the n_e and T_e profiles were naturally matched for the two species when W_{th} was matched by raising the H-NBI auxiliary heating by a factor of 1.6-2 beyond that required for D plasmas [18].

6. Discussion and conclusions

Analysis of the inter-ELM pedestal evolution in a range of JET-ILW H-modes with varying plasma conditions shows that avoiding saturation of the temperature gradient as the pedestal rebuilds in between ELM crashes is crucial to maximizing pedestal performance. Recent non-linear GENE simulations of a sample JET-ILW pedestal at high D_2 gas rate indicate that MTM and ETG turbulence, together with neoclassical transport, is consistent with power balance across the pedestal, with KBMs largely insignificant over the edge transport barrier, except very near the LCFS [19]. As MTMs are driven by the electron temperature gradient, they exhibit the characteristics of a mode that clamps the T_e pedestal evolution, and could therefore be the dominant turbulence in the JET-ILW pedestal as the D_2 gas rate is progressively increased at given input power. Ultimately, edge gyrokinetic analyses and experimental characterization of the turbulence driving the residual pedestal transport inter-ELM are needed in order to advance understanding of the physics at play in JET-ILW pedestals and gain confidence in predictions for ITER and beyond.

Acknowledgements. *This work has been carried out within the framework of the EUROfusion Consortium and has received funding from the Euratom research and training programme 2014-2018 under grant agreement No 633053. The views and opinions expressed herein do not necessarily reflect those of the European Commission*.

References:

[1] MAGGI, C.F., et al., Nucl. Fusion **55** (2015) 113031.
[2] MAGGI, C.F., et al., Nucl. Fusion **54** (2014) 023007.
[3] BELLI, E. and CANDY, J., Plasma Phys. Control. Fusion **50** (2008) 095010.
[4] BELLI, E. and CANDY, J., Plasma Phys. Control. Fusion **54** (2012) 015015.
[5] SAUTER, O., et al., Phys. Plasmas **6** (1999) 2834.
[6] SAUTER, O., et al., Phys. Plasmas **9** (2002) 5140.
[7] HORVATH, L., et al., 43rd EPS Conference on Plasma Physics, Leuven, Belgium, 2016.
[8] SNYDER, P.B., et al, Phys. Plasmas **16** (2009) 056118.
[9] CHAPMAN, I.T., et al., in preparation, Nucl Fusion 2016.
[10] URANO, H., et al., subm Nucl. Fusion 2016.
[11] LEYLAND, M., et al., Nucl. Fusion **55** (2015) 013019.
[12] FRASSINETTI, L., et al., Nucl. Fusion 2016, accepted.
[13] GROEBNER, R.J., et al., Physics of Plasmas **9** (2002) 2134.
[14] HORTON, L.D., et al., Nucl. Fusion **45** (2005) 856.
[15] FRASSINETTI, L., et al., Plasma Phys.Control. Fusion, 2016, accepted.
[16] BEURSKENS, M.N.A., et al., Phys. Plasmas **18** (2011) 056120.
[17] SAARELMA, S., et al., Nucl. Fusion **53** (2013) 123012.

[18] URANO, H., et al., Nucl. Fusion **48** (2008) 045008.
[19] HATCH, D.R., et al., Nucl. Fusion **56** (2016) 104003.

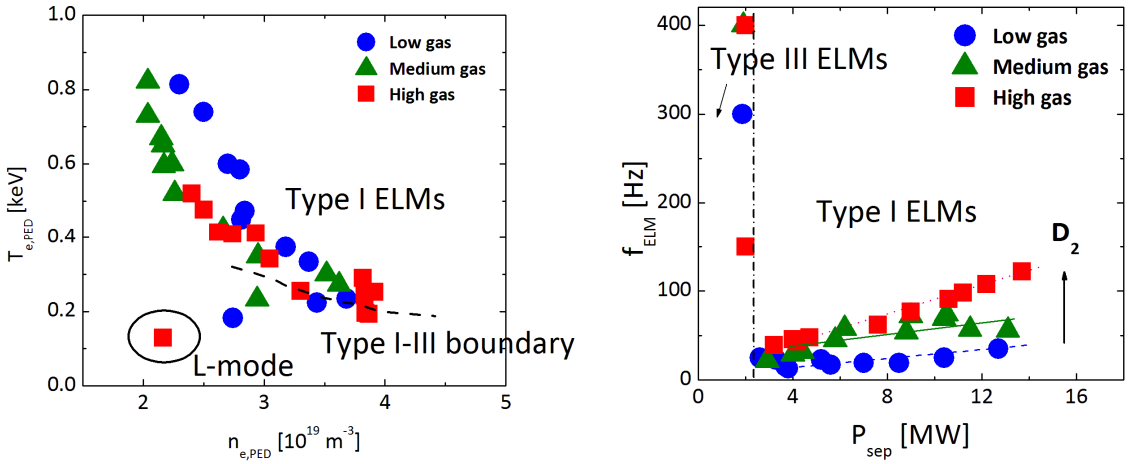

FIG. 1. *$T_{e,PED}$ and $n_{e,PED}$ (a) and ELM frequency vs net power across the separatrix (b) for the dataset of 1.4MA/1.7T power and gas scans at low δ in D plasmas.*

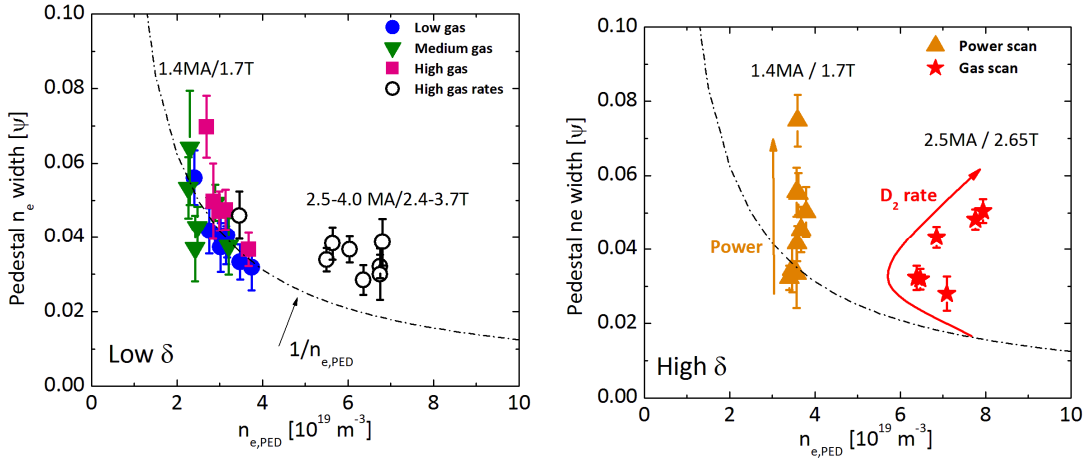

FIG 2. *Comparison of JET-ILW pedestal n_e widths with the assumptions of the neutral penetration model, $\Delta_{ne} \sim 1/n_{e,PED}$: (a) low δ type I ELMy H-modes at 1.4MA/1.7T (power and gas scans) and at higher I_P/B_T and D_2 rates (open black circles); (b) high δ power scan at 1.4MA/1.7T, low D_2 gas rate (orange triangles) and D_2 gas rate at constant power at 2.5MA/2.7T (red stars).*

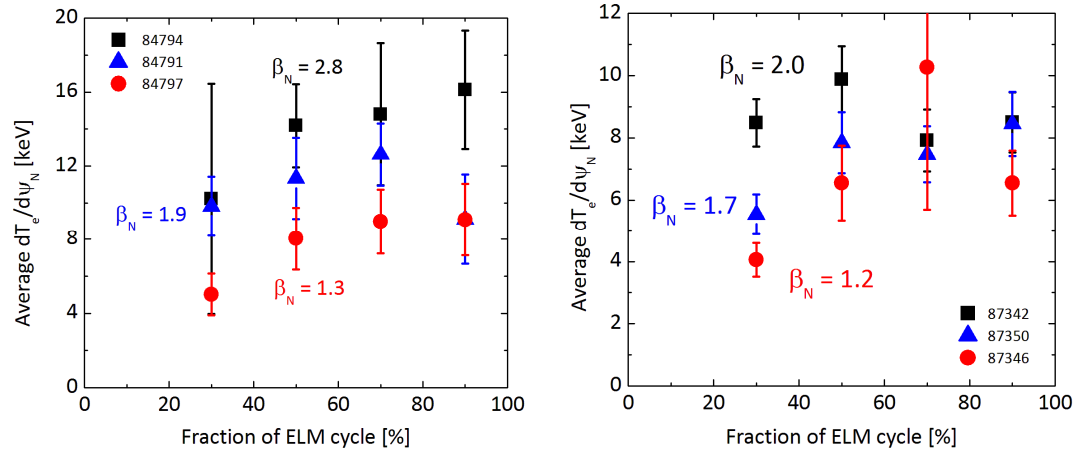

FIG 3. *Pedestal ∇T_e evolution during the type I ELM cycle of the 1.4MA/1.7T power scans at low (a) and high (b) D_2 gas injection.*

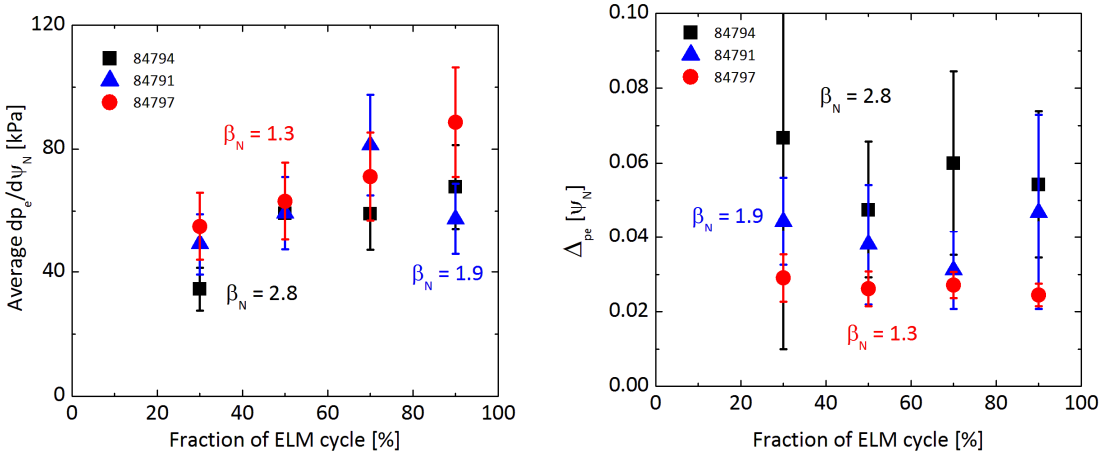

FIG 4. *Pedestal p_e evolution during the type I ELM cycle of the 1.4MA/1.7T power scans at low D_2 gas injection: (a) ∇p_e and (b) Δ_{pe} as a function of normalized ELM fraction.*

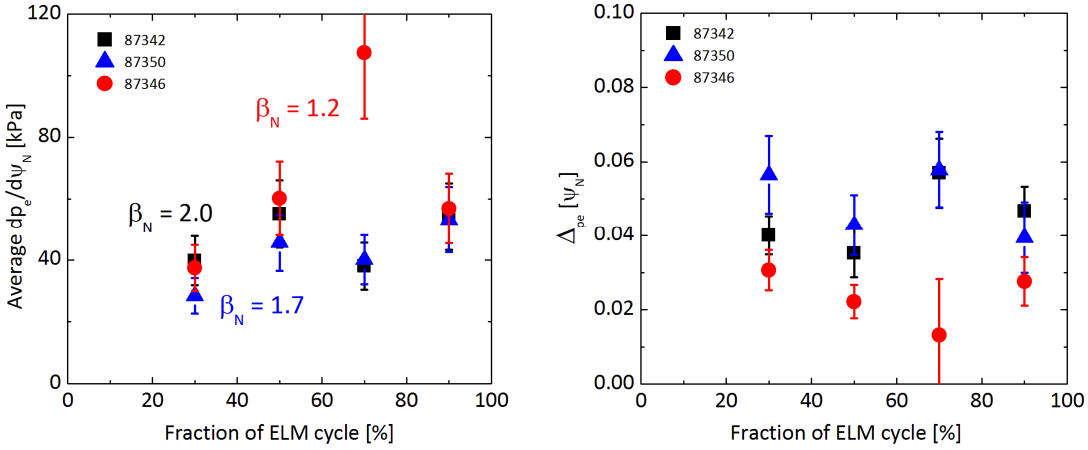

FIG 5. *Pedestal p_e evolution during the type I ELM cycle of the 1.4MA/1.7T power scans at high D_2 gas injection: (a) ∇p_e and (b) Δ_{pe} as a function of normalized ELM fraction.*

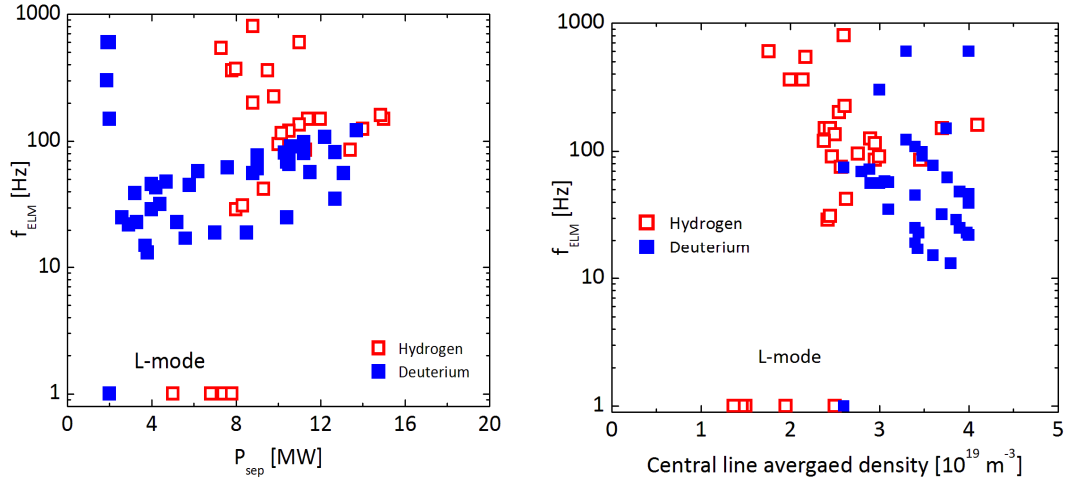

FIG 6. *f_{ELM} vs P_{sep} (a) and f_{ELM} vs plasma density (b) in low δ, H vs D H-modes at 1.4MA/1.7T in JET-ILW.*